CHEMISTRY
AN ASIAN JOURNAL
www.chemasianj.org

## Accepted Article

**Title:** Functionalized Cu-MOF@CNT Hybrid: Synthesis, Crystal Structure and Applicability in Supercapacitors

**Authors:** Shagufi Naz Ansari, Mohit Saraf, Anoop Kumar Gupta, and Shaikh M. Mobin

**To be cited as:** *Chem. Asian J.* 10.1002/asia.201900629

**Link to VoR:** http://dx.doi.org/10.1002/asia.201900629

A Journal of
ACES
Asian Chemical Editorial Society

A sister journal of **Angewandte Chemie** and **Chemistry – A European Journal**

WILEY-VCH

Chemistry - An Asian Journal 10.1002/asia.201900629

# Functionalized Cu-MOF@CNT Hybrid: Synthesis, Crystal Structure and Applicability in Supercapacitors

Shagufi Naz Ansari[†], Mohit Saraf[‡], Anoop K. Gupta[†] and Shaikh M. Mobin[*†‡§]

**Abstract:** *Herein we report synthesis of a new MOF named* ***IITI-1*** *by employing newly design linker $H_2L$ with $Cu(NO_3)_2{\cdot}3H_2O$ in a mixed solvent system of N,N-dimethyl formamide (DMF) and $H_2O$. Further, in order to explore the energy storage application of* ***IITI-1*** *MOF, we have prepared the* ***IITI-1/CNT*** *hybrid by a simple ultrasonication technique. Incorporation of CNT in the layered* ***IITI-1*** *MOF gives rise to enhanced electrolyte accessibility along with the improved electrochemical storage capacity. The electrochemical investigations reveal a high specific capacitance (380 F $g^{-1}$ at 1.6 A $g^{-1}$) with a good rate performance of* ***IITI-1/CNT****. The* ***IITI-1*** *MOF and* ***IITI-1/CNT*** *composite were characterized by PXRD, BET, SEM, and TEM techniques. Moreover,* ***IITI-1*** *MOF was also authenticated by its single crystal X-ray studies.*

Owing to increase in engineering of commercial compact electronic devices, the demand for high energy storage in miniature form has increased enormously.[1-7] In this regard, the electrochemical storage device such as supercapacitors are the most prominent candidate for highly efficient energy storage applications compared to fuel cell [8] and lithium-ion batteries [9], because of its high columbic efficiency, quick charge-discharge process, outstanding environment friendliness, excellent cycling stability and reversibility, which can fulfill the demand for energy consumption and makes them superior to batteries having ordinary power density and cycle life span. To store the energy, supercapacitors exhibits electrical double layer capacitance (EDLC) and pseudo-capacitance-based charge storage mechanisms.[10] Electrode materials for supercapacitors plays important role in the overall performance. Generally, this electrode materials include carbonaceous materials, metal oxides/hydroxides, and conductive polymers [11-12], but have some limitations such as large-scale production, low capacitance in case of carbonaceous materials, poor cycle stability in case of metal oxides/hydroxides, and structural instability as well as fast capacitance deterioration in case of conductive polymers, which restrict their practical applications.[13-16] Thus, construction of electrode materials with durability and low cost remains a great challenge and has attracted significant research efforts for the development of high-performance supercapacitors, that possesses the ability to enhance diffusion kinetics and provide a high accessible surface area.

In this regard, to overcome these limitations, introduction of robust metal-organic frameworks (MOFs) and their composite have shown remarkable performances as electrode material for electrochemical energy storage applications.[17-20] MOFs have witnessed tremendous growth in various potential applications such as electrochemical energy storage/generation,[21,22] sensors,[23,24] catalysis,[25] gas storage/separation[26] owing to their high porosity, robust structure, high specific surface area, conductivity, versatile functionalities and good thermal stability. Furthermore, the direct use of bare MOFs as electrode materials can offer porous skeleton, but they usually exhibit low energy storage performance. For example, Co-based MOFs presented a lower capacitance of around 200 F $g^{-1}$ in LiOH solution, because of low electrical conductivity along with the presence of steric interference to ion insertion.[27] In this regards, assembly of MOFs with graphene, CNTs, carbon black, and so on has emerged as an exceptional strategy for improving the energy storage efficiency.[28] Wen and co-workers fabricated Ni-MOF/CNT composites, which exhibited a brilliant supercapacitor performance due to the synergism between the specific structure of Ni-MOF and high conductivity of CNTs.[28] In this work, CNTs surfaces facilitate the uniform growth of the Ni-MOF, which helped in shortening the pathway of electron transport throughout the charge–discharge process. Additionally, the electronic transportation from active materials towards the current collector was improved by high electronic conductivity of CNTs. Hence, introducing conducting additives such as CNTs in the porous MOF structures can be a viable strategy for advanced energy storage platforms.

In this communication, we have synthesized a newly designed linker ($H_2L$) through a cross-coupling Suzuki reaction of 2,6-dibromo-4-(trifluoromethyl)aniline and 4-(ethoxycarbonyl)phenyl boronic acid, further proceeded by the hydrolysis of diester and its acidification in presence of HCl (**scheme 1**).

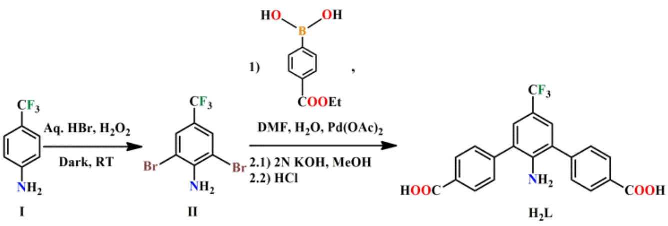

***Scheme 1.*** Synthetic scheme for the ligand, $H_2L$.

Further, a reaction between the $H_2L$ and $Cu(NO_3)_2{\cdot}3H_2O$ in a mixed solvent system of N,N-dimethyl formamide (DMF) and $H_2O$ at room temperature, imparted green coloured crystals with block shape *via* slow evaporation method in ambient conditions. Construction of ***IITI-1 (IITI: Indian Institute of Technology Indore)*** is well illustrated in a schematic representation (**Scheme 2**). Structural analyses shows the robustness of the structure of ***IITI-1***.

---

[†]Discipline of Chemistry, [‡]Discipline of Metallurgy Engineering and Materials Science (MEMS) [§]Discipline for Biosciences and Bio-Medical Engineering (BSBE), Indian Institute of Technology Indore, Simrol, Khandwa Road, Indore 453552, India.
Email: xray@iiti.ac.in

Supporting Information for this article is given via a link at the end of the document.

10.1002/asia.201900629

***Scheme 2.*** Schematic representation for the synthesis of, ***IITI-1***.

Furthermore, a new composite *i.e.* ***IITI-1/CNT*** was formed by blending ***IITI-1*** and CNT via a simple ultra-sonication method. A reasonable schematic diagram presenting the formation of this composite is displayed in **Scheme 3**.

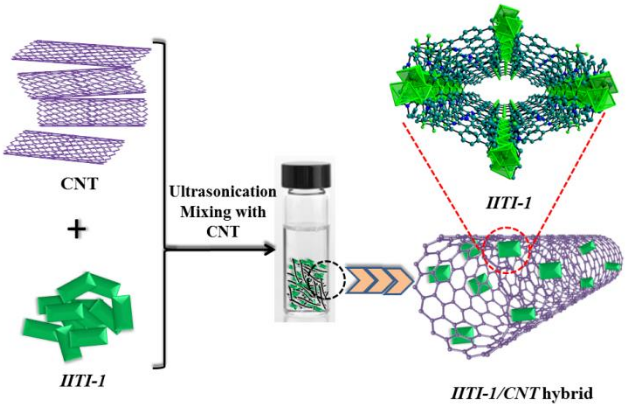

***Scheme 3.*** A reasonable systematic diagram of the formation of ***IITI-1***/CNT hybrid.

***IITI-1*** was characterized by Single crystal x-ray diffraction (SCXRD), PXRD, BET, SEM and TEM analysis. The phase purity of the bulk material of ***IITI-1*** was confirmed by powder X-ray diffraction experiment, which displays that bulk samples are in good agreement with those of corresponding simulated one obtained from SC-XRD data, indicating the presence of crystalline phase (**Figure S1**). PXRD spectrum of ***IITI-1*** represents its crystalline structure and the diffraction pattern of CNT is reliable with the literature. In contrast, PXRD of ***IITI-1/CNT*** reveals that the material is crystalline and contains characteristics of both participating materials without debilitating their properties (**Figure S2**).

***IITI-1*** is a well-defined two dimensional (2-D) layered coordination polymer. Its asymmetric unit contains one copper(II) atom, one DMF molecule and one deprotonated $H_2L$. Single-crystal X-ray diffraction analysis (**Table S1**) indicated that ***IITI-1*** crystallized in the monoclinic *C*2/*c* space group. Each Cu ion is coordinated by four carboxylate oxygen atoms from $H_2L$ ligands in a square pyramidal molecular geometry at basal positions and at the apical position it is coordinated to one oxygen atom from DMF molecule (**Figure 1a**). The supramolecular framework is constructed of 4-connected paddle-wheel dinuclear $Cu_2(COO)_4$ secondary building units (SBUs) with a Cu···Cu distance of 2.634(2) Å (**Figure S3**). Each $H_2L$ ligand coordinates to four Cu(II) atoms through two carboxylate groups claiming $\mu_2$-$\eta^1$:$\eta^1$ and $\mu_2$-$\eta^1$:$\eta^1$ coordination modes, respectively. The spanning range of calculated Cu···O bond measurements range from 1.957(4) to 2.199(7) (Å) to form a 2-D layered framework (**Figure 1b**). All measured bond distances (**Table S2**) were comparable to literature values.[29]

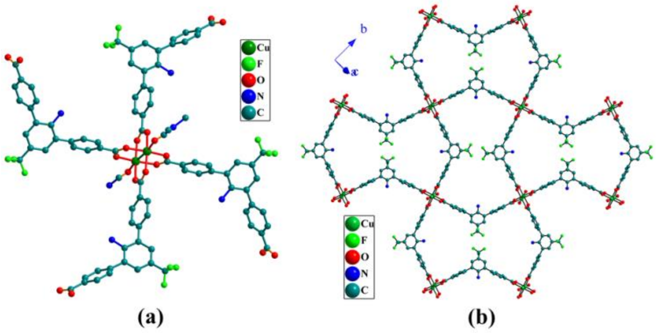

***Figure 1.*** Ball & stick model showing (a) the coordination environment around Cu(II) ion in ***IITI-1***, (b) the 2-D sheet between ab axis; Color code: Cu: green; O: red; N: blue; and C: olive (hydrogen atoms are omitted for clarity).
.

The infinite 2-D layers of ***IITI-1*** are stacked in a slipped fashion in b direction (**Figure 2a**) driven by CH···π interactions and hydrogen bondings (C-H···O interaction) resulting in the formation of a 3-D supramolecular layered framework forming stable 1-D pore channels along c axis with effective dimensions of 19.901 Å × 14.022 Å decorated with $NH_2$ and $CF_3$ group (**Figure 2b**), through which the permeation of electrolytes could be easily allowed. CH···π interactions are present in framework with the distance C17–H···π=2.873 Å and ∠C14–H14···π=109.08˚.

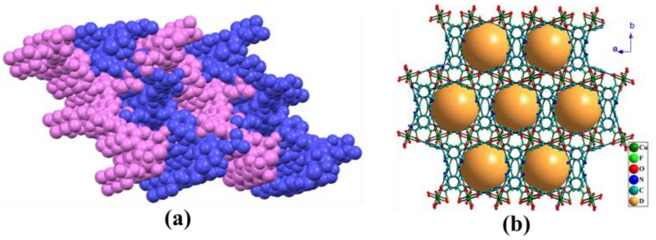

***Figure 2.*** (a) Space fill model displaying the layered stacking in ***IITI-1***, (b) Ball & stick model showing cages in the supramolecular 3D framework along c-axis. Color code: Cu: green; O: red; N: blue; and C: olive (hydrogen atoms are omitted for clarity).

The BET surface area for ***IITI-1***, **CNT** and ***IITI-1*/CNT** and their porosity information were recorded by measuring and analysing the sorption isotherms at 77 K using $N_2$ gas. The results display type IV adsorption isotherm profile for ***IITI-1*** and type III adsorption isotherm profile for CNT and ***IITI-1*/CNT**. The

10.1002/asia.201900629

evaluated BET surface areas of ***IITI-1***, **CNT** and ***IITI-1*/CNT** are 986.764 m$^2$ g$^{-1}$, 421.491 m$^2$ g$^{-1}$ and 185.008 m$^2$ g$^{-1}$, respectively (**Figure S4–S6†**). The respective plots for BJH pore size distribution are presented in the insets of Fig. S4–S6.† The morphology and structure of prepared samples were perceived by SEM and TEM techniques. SEM images of ***IITI-1*** display irregular block shaped structure of size varying between 1-10 µm (**Figure S7a**), whereas both block shaped crystals as well as typical nanotubes of carbon are present in the ***IITI-1*/CNT** (**Figure S7c,d).** These observations were further confirmed in TEM results, where block shaped particles were observed for ***IITI-1*** (**Figure 3a,b**), distinct nanotubes were observed for CNT (**Figure 3c,d**), and an uniform enwrapping of CNTs by ***IITI-1*** were found in ***IITI-1*/CNT** (**Figure 3e,f**). The SEM and TEM results verify the hybrid formation as both types of structures were present in the material.

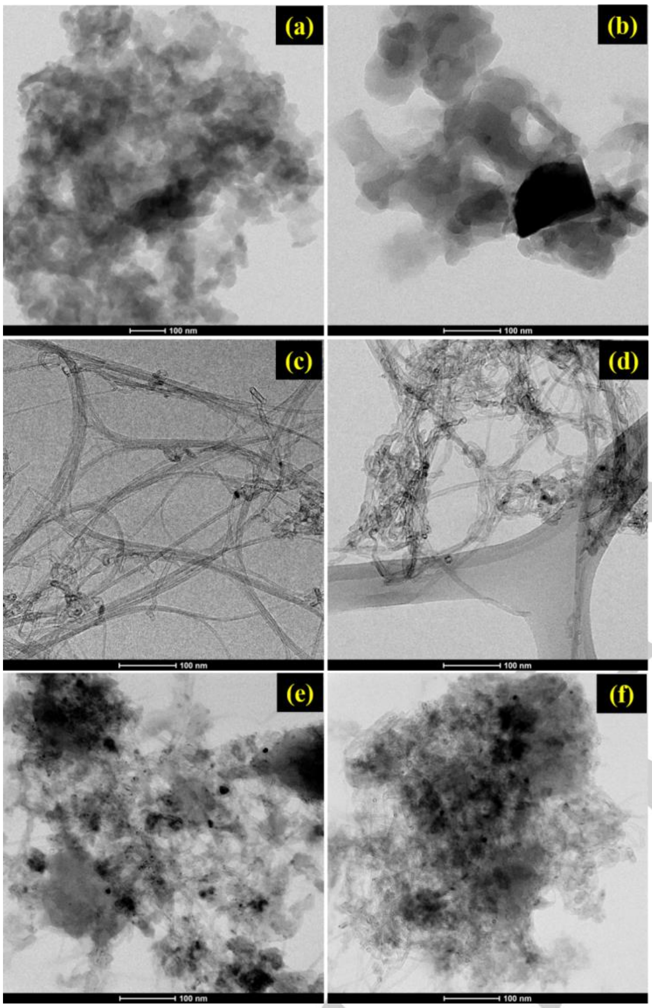

***Figure 3.*** TEM images of (a,b) ***IITI-1***, (c,d) CNT, and (e,f) ***IITI-1/CNT***.

### Supercapacitor properties of *IITI-1*, CNT and *IITI-1*/CNT

The electrochemical investigations of ***IITI-1*/CNT** composite were carried out using a three-electrode cell in 1 M $Na_2SO_4$ aqueous electrolyte in the absence of any commercial binders. This approach of binderless preparation of working electrode can be cost-effective for real-world device applications. The drop-cast electrodes of ***IITI-1***, CNT and ***IITI-1*/CNT** were denoted as ***IITI-1***/GCE, CNT/GCE and ***IITI-1*/CNT**/GCE, respectively and their supercapacitor properties were compared systematically by cyclic voltammetry (CV) and galvanostatic charge–discharge (GCD) techniques.

In the initially conducted experiments, CV profiles of all three electrodes were compared at 100 mV s$^{-1}$, which shows a remarkably enhanced charge propagation and integrated area under the curve for ***IITI-1***/CNT/GCE compared to other electrodes (**Figure 4a**). This observation suggests a high specific capacitance of composite over individual materials.

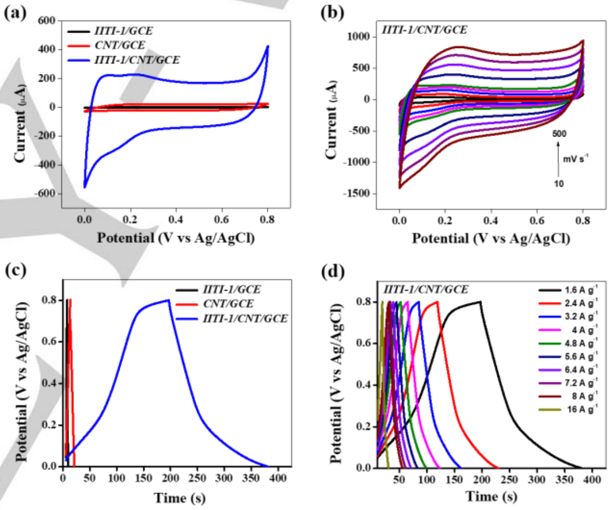

***Figure 4.*** (a) Comparison of CV profiles of ***IITI-1***/GCE, CNT/GCE and ***IITI-1***/CNT/GCE at 100 mV s$^{-1}$, (b) CV profiles of ***IITI-1***/CNT/GCE at different scan rates (10-500 mV s$^{-1}$), (c) comparison of GCD profiles of ***IITI-1***/GCE, CNT/GCE and ***IITI-1***/CNT/GCE at 1.6 A g$^{-1}$, and (d) GCD profiles of ***IITI-1***/CNT/GCE at different current densities (1.6-16 A g$^{-1}$). (Electrolyte: 1M $Na_2SO_4$).

The CV profiles of ***IITI-1***/GCE exhibits a lethargic charge transfer process with a very less induced current (**Figure S16a**). Moreover, CV profiles at different scan rates (10-500 mV s$^{-1}$) do not present any ideal rectangular CV curves, which suggest the absence of double layer capacitive process and appearance of peaks recommends the possibility of pseudocapacitive process. In contrast, CNT/GCE, being a carbon material, presents nearly rectangular CV profiles at different scan rates (**Figure S16b**) with good charge propagation compared to ***IITI-1***/GCE, however, it is still insufficient to generate very high specific capacitance. The enhanced current response of CNT/GCE over ***IITI-1***/GCE can be assessed by comparing the y-axes of **Figure S16a and b**. Looking into CV profiles, it is observed that in comparison with ***IITI-1***/GCE and CNT/GCE, ***IITI-1***/CNT/GCE exhibits

10.1002/asia.201900629

massively promoted charge propagation and storage capacity, signifying the benefit of elaborated MOF architecture with the support of CNTs (**Figure 4b**). Moreover, CV profiles of ***IITI-1***/CNT/GCE attain quasi-rectangular behavior, which shows a good synergy of CNT with MOF. The continuously enhanced CV integrated area under the curves for ***IITI-1***/CNT/GCE along with the amplified current response without any noticeable signal loss at higher scan rates, reveal its good charge storage characteristics and high rate ability. This escalated charge storage and related properties is the outcome of the positive synergistic properties between 2-D Cu-MOF and highly conducting CNT.[2,7] In conclusion, the promoted charge storage characteristics in ***IITI-1***/CNT/GCE can be assigned as a synergistic alliance of pseudocapacitive ***IITI-1***/GCE and double layer capacitive CNT/GCE.

The observed synergy between MOF and CNT was further observed in galvanostatic charge–discharge (GCD) observations. The comparison of GCD profiles of all three electrodes is presented in **Figure 4c**, which shows greatest discharge time in case of ***IITI-1***/CNT/GCE. This observation suggests highest specific capacitance of ***IITI-1***/CNT/GCE over other electrodes. ***IITI-1***/GCE displays a non-ideal triangular shape of GCD curves owing to possible dominance of redox process, which is a characteristic of pseudocapacitance (**Figure S16c**). Furthermore, the sluggish charging-discharging process was accompanied with IR drop (potential drop) due to internal resistance. This IR drop keeps on growing with increasing current densities, which may be assigned due to electronic hindrance associated with electroactive materials and ionic resistance correlated to conductivity of electrolyte and mobility of ions, and results in low charge storing efficiency.[2,12,16] Similar observations were noticed for CNT/GCE, where the value of IR drop was comparably larger than ***IITI-1***/GCE at each current densities (**Figure S16d**). However, this potential drop remains disappeared in ***IITI-1***/CNT/GCE at each current densities indicating the minimized internal resistance (**Figure 4d**), which shows its good conductivity and excellent charge storage efficiency. Furthermore, the GCD profiles of ***IITI-1***/CNT/GCE were somewhat triangular due to a healthy alliance between MOF and CNT. The GCD curve profiles at each current density displays the highest discharge time for ***IITI-1***/CNT/GCE over other electrodes (**Figure 4d),** which is the confirmation of the largest specific capacitance of hybrid over ***IITI-1*** and CNT. These results are in line with those obtained through CV. The calculated specific capacitances for ***IITI-1***/CNT/GCE at current densities of 1.6, 2, 2.4, 2.8, 3.2, 3.6, 4, 8 and 16 are 380, 330, 312, 285, 276, 273, 264, 261, 260 and 240 F $g^{-1}$, respectively. The calculated areal capacitance at 0.282 mA $cm^{-2}$ was 0.067 F $cm^{-2}$ and at high current density of 2.8 mA $cm^{-2}$ was 0.044 F $cm^{-2}$. Due to insufficient utilization of active ionic species, the energy storage capability reduces at higher current densities as shown by the plotted graph of applied current densities and the obtained specific capacitance (**Figure 5a**).[2,16] A good rate performance was observed for ***IITI-1***/CNT/GCE, which can retain 63.15% of its initial capacitance up to 16 A $g^{-1}$ [14] The specific capacitance and other performance parameters are not given for ***IITI-1***/GCE and CNT/GCE, as they are considerably lower than ***IITI-1***/CNT/GCE, indicated in both CV and GCD results. The high performance of ***IITI-1***/CNT/GCE or ***IITI-1***/*CNT* can be assigned to the following factors: (i) the precisely defined porous structure of ***IITI-1*** stimulates the electrolyte access to the electrolyte, (b) the ***IITI-1*** structure wrapped by the CNT can function as a current collector along with a long-route charge carrier throughout the process of charge–discharge mode, and (c) the electron transportation can be improved by the high electronic conductivity of CNT via decreasing equivalent series resistance. As one of the essential requirements and important features of supercapacitors, the cycling stability test was also performed for ***IITI-1***/CNT/GCE at 16 A $g^{-1}$ (**Figure 5b**). A long life cycle is obtained with 63.63% retention of initial capacitance up to 4000 cycles, validating its superior long-lasting efficiency. The inset of **Figure 5b** presents first 25 GCD cycles, which show excellent reversibility. Such good cyclic efficiency of hybrid is the outcome of stable and robust composite formation due to a proper association between ***IITI-1*** and CNT, which alleviate the requirement of any commercial expensive binders.

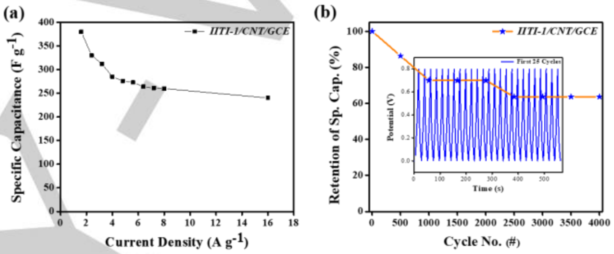

***Figure 5.*** (a) Plot of calculated specific capacitance against current densities, (b) cycling stability analysis test for ***IITI-1***/CNT/GCE up to 4000 cycles, where inset shows first 25 cycles (Electrolyte: 1M $Na_2SO_4$).

The comparison of supercapacitor performance of ***IITI-1***/CNT with some advanced MOF structures and hybrids have been displayed in **Table S3**. Several considerations have been taken into account to conclude that ***IITI-1***/CNT, a hybrid structure of ***IITI-1*** and CNT, is an emerging aspirant for next generation supercapacitors.

Electrochemical Impedance Spectroscopy (EIS) experiments were used to further examine the charge transfer characteristics of ***IITI-1***/GCE and ***IITI-1***/CNT/GCE electrodes. A single semicircle was largely observed in the Nyquist plots from the EIS spectrum, corresponding to one impedance element. This was correspondingly mapped to a simple RC series circuit with a series resistance with the capacitance replaced by a Constant Phase Element (CPE) due to non-ideal behavior of the plot,[30] assumed to be due to the double-layer phenomena. The mapped values according to the circuit in inset are shown in (**Table S4, Figure S17**). It is observed that $R_{ct}$ value actually increases with the addition of CNT, but this is attributed to the participation of CNT in the redox process, leading to higher capacitance values in the capacitance tests[31]. The value of ϕ is 0.7, which is leaning towards capacitance characteristic for the Nyquist impedance. After cycling, there is a significant rise in the charge transfer resistance $R_{ct}$, which is attributed to structural degradation.[32]

In summary, a simple ultrasonication technique has been employed for the preparation of ***IITI-1/CNT*** hybrid. Incorporation of CNT in the layered ***IITI-1*** give rise to synergistically improved electrochemical energy storage efficiency, which is evident in noteworthy high specific capacitance and good rate performance of ***IITI-1/CNT***. From the results, it can be presumed that the precisely defined porous structure of ***IITI-1*** stimulates the electrolyte access to the active sites, and the high electronic conductivity of CNTs can accelerates the electronic transportation, which contribute immensely in delivering high electrochemical performance. The present work highlights the importance of MOF/carbonaceous materials to be promising supercapacitor electrode materials.

**Experimental Section**

**Synthesis of $H_2$L**

The synthesis of functionalized linker was achieved according to previous literature [29] and given in the **SI (Figure S8-S15)**.

**Synthesis of $\{[Cu(L)(DMF)]\cdot(Solvent)_x\}_n$ or (*IITI-1*)**

$H_2$L (20 mg, 0.05 mmol) was dissolved in DMF (4 mL) and mixed with $Cu(NO_3)_2\cdot3H_2O$ (35 mg, 0.15 mmol,) with further addition of $H_2O$ (1ml) and conc. HCl (1 drop). Clear solution was obtained. The mixture was placed in a conical flask and placed for slow evaporation at room temperature. Green-colored block-shaped crystals of ***IITI-1*** were obtained in 7 days with 52% yield. FT-IR (KBr pellets, cm−1): 3447 (broad), 1706(m), 1609 (s), 1540 (m), 1404 (s), 1359 (s), 1262(s), 1179 (m), 1156 (s), 1109 (s), 1034 (s), 900 (s), 866 (s), 791 (m), 716 (s).

**Synthesis of *IITI-1*/CNT Hybrid**

The CNTs were purchased and utilized without any modification. The composite of ***IITI-1*** and CNT was prepared using the ultra-sonication assisted technique by acquiring them in 1:1 ratio (wt%). In this method, appropriate amount of CNT was dispersed in a solution of ***IITI-1*** in ethanol by doing sonication for 1 hr and then dried by rotary evaporation. The obtained black colored powder represents the composite of ***IITI-1*** and CNT and termed as ***IITI-1*/CNT**.

## Acknowledgements

Authors are grateful to the Sophisticated Instrumentation Centre (SIC), IIT Indore for providing characterization facilities. S.N.A. and M.S. are thankful to MHRD, New Delhi, India for providing Teaching Assistantship (TA) research fellowship. A.K.G. gratefully thanks to IIT Indore for a research fellowship. S.M.M. thanks SERB-DST (Project No. EMR/2016/001113) and CSIR (Project No. 01(2935)/18/EMR-II), New Delhi and IIT Indore India for financial support. S.N.A. thanks SAIF, IIT Bombay for TEM measurements. This work made use of the I19 beamlines at the Diamond synchrotron, U.K. (experiment MT21377-1).

**Keywords:** supercapacitor, ***IITI-1*** MOF, CNT, specific capacitance, cyclic voltammetry

1. J. Yan, L. Yang, M. Cui, X. Wang, K. J. Chee, V. C. Nguyen, V. Kumar, A. Sumboja, M. Wang, P. S. Lee, *Adv. Energy Mater*. **2014**, *4*, 1400781
2. M. Saraf, R. Rajak, S. M. Mobin, *J. Mater. Chem. A* **2016**, *4*, 16432-16445.
3. Z.-X. Li, B.-L. Yang, K.-Y. Zou, L. Kong, M.-L.Yue, H.-H. Duan, *Carbon* **2019**, *144*, 540-548.
4. (a) D. W. Wang, F. Li, M. Liu, G. Q. Lu, H. M. Cheng, *Angew. Chem. Int. Ed*. **2008**, *120*, 379-382; (b) Q.-L. Zhu, P. Pachfule, P. Strubel, Z. Li, R. Zou, Z. Liu, S. Kaskel, Q. Xu, *Energy Storage Mater*. **2018**, *13*, 72-79; (c) B. Fang, J. H. Kim, M.-S. Kim, A. Bonakdarpour, A. Lam, D. P. Wilkinson, J.-S. Yu, *J. Mater. Chem.* **2012**, *22*, 19031-19038; (d) D. Sheberla, J. C. Bachman, J. S. Elias, C. J. Sun, Y. Shao-Horn, M. Dinca, *Nat. Mater*. **2016**, *16*, 220.
5. R. Zhang, J. Ding, C. Liu, E.-H. Yang, *ACS Appl. Energy Mater*. **2018**, *1*, 2048-2055.
6. D. P. Dubal, K. Jayaramulu, J. Sunil, Š. Kment, P. Gomez‐Romero, C. Narayana, R. Zbořil, R. A. Fischer, *Adv. Funct. Mat.* **2019**, *29*,1900532.
7. R. Rajak, M. Saraf, S. M. Mobin, *J. Mater. Chem. A* **2019**, *7*, 1725-1736.
8. E. Kjeang, R. Michel, D. A. Harrington, N. Djilali, D. Sinton, *J. Am. Chem. Soc*. **2008**, *130*, 4000-4006.
9. S. Jiang, Y. Lu, Y. Lu, M. Han, H. Li, Z. Tao, Z. Niu, J. Chen, *Chem. Asian J*. **2018**,*13*,1379 -1385.
10. (a) P. Simon, Y. Gogotsi, B. Dunn, *Science* **2014**, *343*, 1210, (b) M. Saraf, K. Natarajan, S M Mobin, *ACS Sustain. Chem. Eng*. **2018**, *6*, 10489–10504;
11. A. S. Levitt, M. Alhabeb, C. B. Hatter, A. Sarycheva, G. Dion, Y. Gogotsi, *J. Mater. Chem. A* **2019**, *7*, 269-277.
12. M. Saraf, K. Natarajan, S. M. Mobin, *ACS Appl. Mater. Interfaces*, 2018, 10, 16588-16595.
13. M. K. Aslam, S. S. A. Shah, S. Li, C. Chen, *J. Mater. Chem. A* **2018**, *6*, 14083-14090.
14. R. Rajak, M. Saraf, A. Mohammad, S. M. Mobin, *J. Mater. Chem. A*, **2017**, *5*, 17998-18011.
15. R. R. Bi, X. L. Wu, F. F. Cao, L. Y. Jiang, Y. G. Guo, L. J. Wan, J. Phys. Chem. C **2010**, *114*, 2448.
16. M. Saraf, K. Natarajan, S. M. Mobin, *RSC Adv*., **2017**, *7*, 309−317.
17. N. Stock, S. Biswas, *Chem. Rev*. **2011**, *112*, 933.
18. (a) R. R. Salunkhe, Y. V. Kaneti, J. Kim, J. H. Kim, Y. Yamauchi, *Acc. Chem. Res.* **2016**, *49*, 2796-2806 (b) P. Nugent, Y. Belmabkhout, S. D. Burd, A. J. Cairns, R. Luebke, K. Forrest, T. Pham, S. Ma, B. Space, L. Wojtas, M. Eddaoudi, M. J. Zaworotko, *Nature* **2013**, *495*, 80-84; (c) S. Bureekaew, S. Horike, M. Higuchi, M. Mizuno, T. Kawamura, D. Tanaka, N. Yanai, S. Kitagawa, *Nat. Mater*. **2009**, *8*, 831-836; (d) P. Horcajada, R. Gref, T. Baati, P. K. Allan, G. Maurin, P. Couvreur, G. F´erey, R. E. Morris, C. Serre, *Chem. Rev*. **2012**, *112*, 1232-1268.
19. M. Du, Mi. Chen, X. G. Yang, J. Wen, X. Wang, S. M. Fang, C. S. Liu, *J. Mater. Chem. A* **2014**, *2*, 9828.
20. C. Ye, Q. Qin, J. Liu, W. Mao, J. Yan, J. Yan, Y. Wang, J. Cui, Q. Zhang, L. Yang, Y. Wu, *J. Mater. Chem*. **2019**, *7*, 4998-5008.
21. K. M. Choi, H. M. Jeong, J. H. Park, Y. B. Zhang, J. K. Kang, O. M. Yaghi, *ACS Nano* **2014**, *8*, 7451.
22. K. Natarajan, A. K Gupta,. S. N. Ansari, M. Saraf, S. M. Mobin, *ACS Appl. Mater. Interfaces* **2019**, *11*, 13295-13303.
23. A. K. Gupta, K. Tomar, P. K. Bharadwaj, CrystEngComm **2017**, 19, 2253-2263.
24. A. K. Gupta, K. Tomar, Parimal K. Bharadwaj, *New J. Chem*. **2017**, *41*, 14505-14515.
25. (a) A. K. Gupta, D. De, R. Katoch, A. Garg, P. K. Bharadwaj, *Inorg. Chem*. **2017**, *56*, 4697-4705. ; (b)L. Ma, C. Abney, W. Lin, *Chem.*

*Soc. Rev*. **2009**, *38*, 1248-1256. (c) A. K. Gupta, D. De, K. Tomar, P. K. Bharadwaj, *Dalton Trans*. **2018**, *47*, 1624-1634

26. L. Li, R. B. Lin, R. Krishna, H. Li, S. Xiang, H. Wu, J. Li, W. Zhou, B. Chen, *Science* **2018**, *362*, 443-446.
27. D. Y. Lee, D. V. Shinde, E. K. Kim, W. Lee, I. W. Oh, N. K. Shrestha, J. K. Lee, S. H. Han, *Microporous Mesoporous Mate*r., **2013**, *171,* 53.
28. P. Wen, P. Gong, J. Sun, J. Wang, S. Yang, *J. Mater. Chem. A* **2015**, *3*, 13874-13883.
29. A. K. Gupta, D. De, P. K. Bharadwaj *Dalton Tran*s. **2017**, *46*, 7782-7790.
30. J. Tymoczko, W. Schuhmann, A. S. Bandarenka*, Electrochemistry Communications***, 2013***, 27*, 42-45.
31. H. S. Jang, C. J. Raj, W. –G. Lee, B. C. Kim, K. H. Yu, *RSC Adv*., **2016,** *6*, 75376.
32. T. Wang, Q. Lea, J. Zhang, Y. Zhang, W. Li, *Electrochimica Acta* 2017, 253, 311–318.

## Entry for the Table of Contents

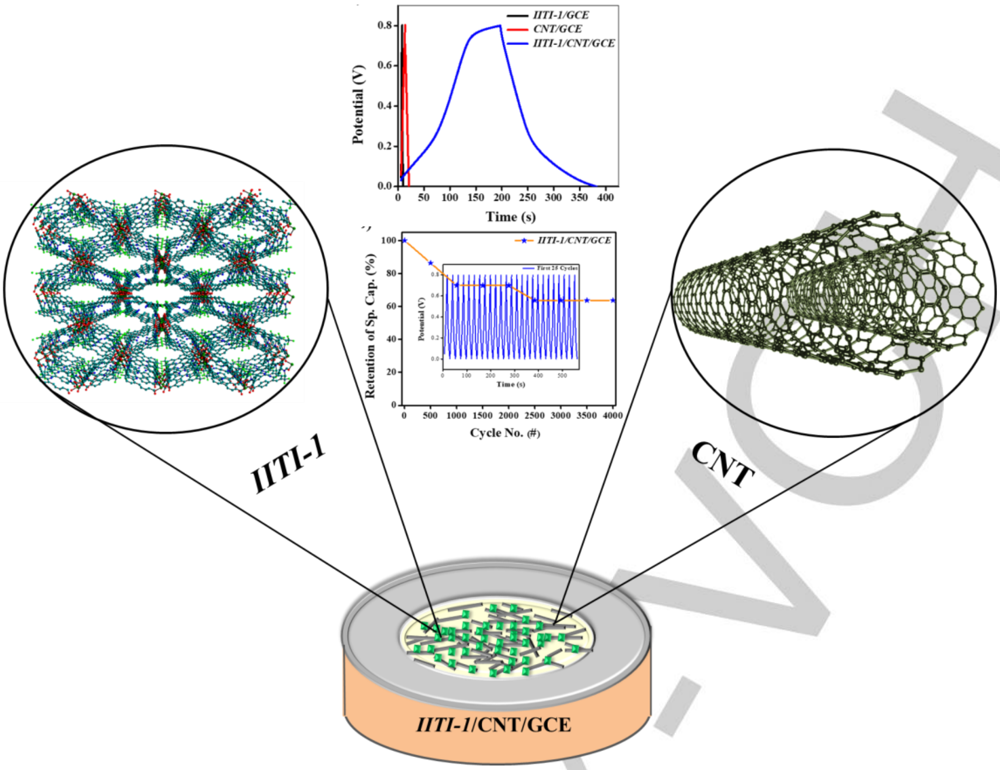

A functionalized layered Cu-MOF (***IITI-1***) has been synthesized in a facile manner. Incorporation of CNT in this layered ***IITI-1MOF*** give rise to synergistically improved electrochemical energy storage efficiency.

*Shagufi Naz Ansari†, Mohit Saraf‡, Anoop K. Gupta† and Shaikh M. Mobin**

*Page No. - Page No.*

**Functionalized Cu-MOF@CNT Hybrid: Synthesis, Crystal Structure and High-Performance Supercapacitors**